Energy & Environmental Science

Dynamic Article Links

Cite this: *Energy Environ. Sci.*, 2012, **5**, 9107

www.rsc.org/ees

PAPER

Metal–organic frameworks with potential for energy-efficient adsorptive separation of light hydrocarbons†

Yabing He,[a] Rajamani Krishna*[b] and Banglin Chen*[a]

Received 15th July 2012, Accepted 9th August 2012
DOI: 10.1039/c2ee22858k

The separation of hydrocarbons with carbon numbers in the 1–3 range is of great significance in the purification of natural gas, production of ethylene and propylene with the required 99.5%+ purity levels as feeds to polymerization reactors, and separation of ethyne from mixtures with ethylene. In this study the performances of a total of 19 different MOFs, carefully selected to span a wide range of functionalities, were evaluated for a variety of separation tasks. For all separation tasks investigated, MOFs with high density of open metal sites, **CoMOF-74**, **MgMOF-74**, and **FeMOF-74**, have significantly better separation potential than other MOFs, ZIFs or zeolites that have been suggested in the literature. Of particular significance is the possibility offered by **CoMOF-74**, **MgMOF-74**, and **FeMOF-74** for "fractionating" a 6-component $CH_4/C_2H_2/C_2H_4/C_2H_6/C_3H_6/C_3H_8$ mixture to yield individual pure components. Such separations are likely to have a significant industrial impact, resulting in significant energy savings when compared to current technologies that rely on distillation.

Introduction

C_1 to C_3 light hydrocarbons, CH_4, C_2H_2, C_2H_4, C_2H_6, C_3H_6, and C_3H_8, are very important energy resources and raw chemicals. For example, natural gas, whose main component is methane, has been considered as the most promising alternative fuel for future vehicle transportation; while both ethylene and propylene are important chemicals for the manufacture of polymers such as polyethylene, polypropylene, polyvinyl chloride, polyester, polystyrene as well as other organic chemicals. In order to fully utilize these light hydrocarbons, it is essential to have high quality and purity of such basic chemicals; thus, separations of these light hydrocarbons are very important industrial processes. The traditional separation technology of the cryogenic distillation, which is based on their different vapor pressures and thus boiling points, is very energy-intensive. Among several new

[a]*Department of Chemistry, University of Texas at San Antonio, One UTSA Circle, San Antonio, Texas 78249-0698, USA. E-mail: Banglin.Chen@utsa.edu*
[b]*Van't Hoff Institute for Molecular Sciences, University of Amsterdam, Science Park 904, 1098 XH Amsterdam, The Netherlands. E-mail: r.krishna@uva.nl*

† Electronic supplementary information (ESI) available: A document containing: (a) structural and synthesis details for various MOFs; (b) details of experimental isotherm data measurements and uptake data; (c) isotherm fit parameters for all pure component isotherms of the materials considered in this work; (d) details of the numerical procedure used in breakthrough calculations; (e) validation of the breakthrough simulation methodology by comparison with published experimental data from a variety of literature sources; (f) IAST calculation results of selectivity and capacity for all mixtures; (g) breakthrough calculation results for all mixtures considered in this work; (h) video animations showing 6-component pulse breakthrough simulations for **MgMOF-74**. See DOI: 10.1039/c2ee22858k

Broader context

While CO_2 capture in pre- and post-combustion processing garners a lot of current research interest in the development of novel materials such as metal–organic frameworks (MOFs), there is a much wider scope for using MOF adsorbents in other processes of current and future industrial interest. The main focus of this article is to demonstrate the significant advantages of MOFs with open metal sites, for separation of light hydrocarbon mixtures, with C numbers in the 1–3 range, in a variety of contexts that are important in the petrochemical and energy sectors. Specifically, **MgMOF-74**, **CoMOF-74**, and **FeMOF-74** have a strong propensity to bind, with high selectivity, alkynes and alkenes. This selective binding of double and triple bonds with the metal atoms leads to the possibility of separating ethylene–ethane, propylene–propane, and ethyne–ethylene mixtures, all of which are of great importance in the petrochemical industries. Furthermore, we demonstrate for the first time in the published literature the potential of **MgMOF-74**, **CoMOF-74**, and **FeMOF-74** for *fractionation* of a 6-component $CH_4/C_2H_2/C_2H_4/C_2H_6/C_3H_6/C_3H_8$ mixture, which is of great significance in natural gas processing.

energy-efficient technologies for such important hydrocarbon separations, adsorptive separation is one of the most promising ones, so a variety of microporous adsorbents have been examined for separations of these light hydrocarbons.

Microporous metal–organic frameworks (MOFs) have been rapidly emerging as very useful materials for separations of small gas molecules.[1–23] They can be readily self-assembled from metal ions and/or metal-containing clusters with organic linkers. Because the pores within such microporous MOFs can be tuned to maximize their size-selective sieving effects and the pore surfaces can be functionalized to direct their specific recognitions of small molecules, microporous MOFs are very unique materials for separations. In fact, a variety of microporous MOFs have been explored for their diverse gas separations such as separations of CO_2/CH_4,[2,4,23–25] alkane and xylene isomers.[26–34]

Adsorptive separation of C_1 methane from C_2 and C_3 hydrocarbons is comparatively easier given the fact that methane is the smallest molecule and therefore has weaker interactions with microporous MOF adsorbents.[25,35–38] Separations of C_2H_2/C_2H_4, C_2H_4/C_2H_6, and C_3H_6/C_3H_8, however, are very difficult, because these individual pair molecules have comparable sizes. In fact, only recently have a few microporous MOFs been targeted for these very challenging hydrocarbon separations.[39–57] The four (CH_4, C_2H_2, C_2H_4, and C_2H_6) and six (CH_4, C_2H_2, C_2H_4, C_2H_6, C_3H_6, and C_3H_8) component separations are even much more challenging.[43,58] Highly efficient separations of these mixtures of light hydrocarbons into their high-purity individual components can significantly save the energy cost, and thus are heavily in need. In this study, we examine the potential of microporous MOFs for adsorptive separations of these light hydrocarbons. For this purpose, 19 microporous MOFs of different pore structures, porosities, and surfaces have been selected to establish their hydrocarbon sorption isotherms, and to examine their potential for separations of light hydrocarbons through simulated breakthrough experiments. They have also been compared with the excellent performing microporous adsorbents, **NaX**,[59,60] **NaETS-10**,[61] and **FeMOF-74**.[43]

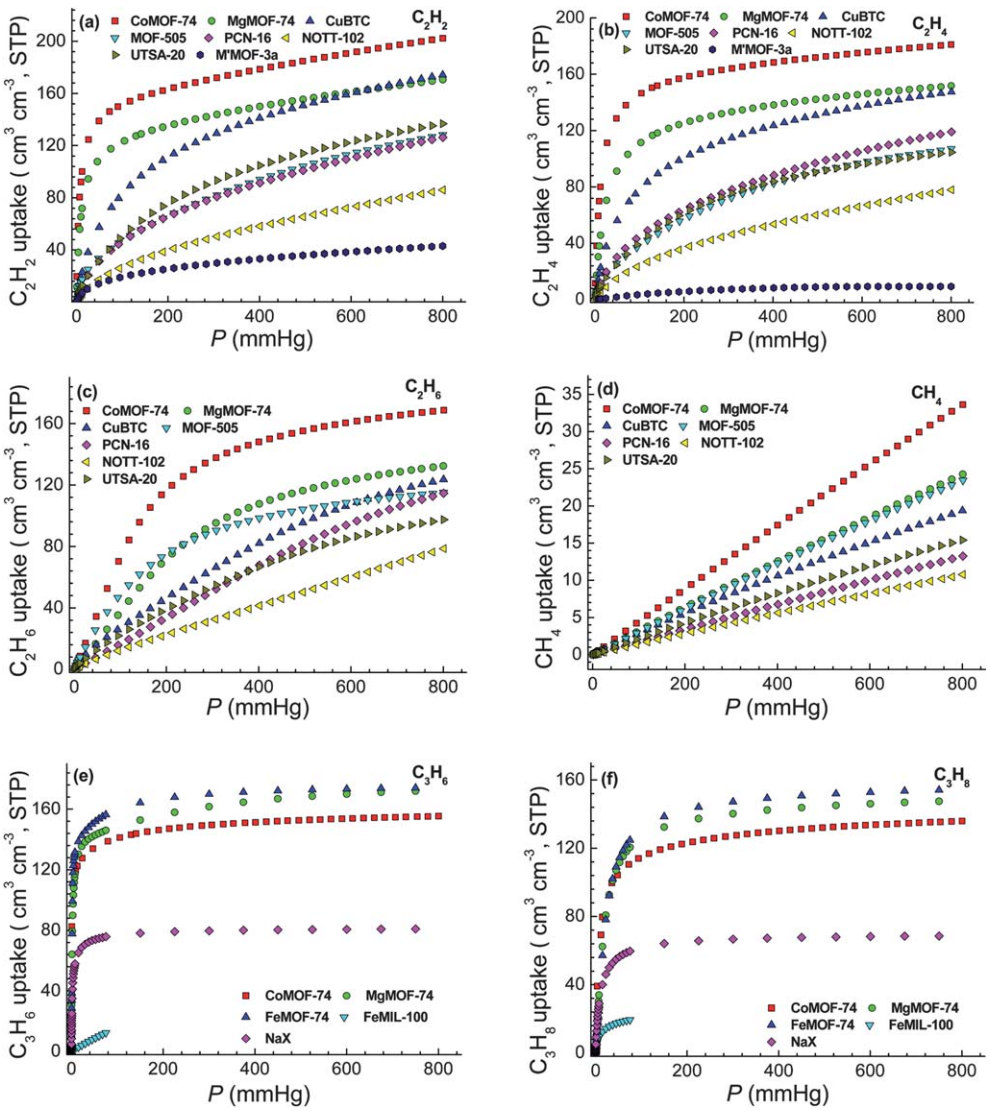

Fig. 1 (a) C_2H_2, (b) C_2H_4, (c) C_2H_6, (d) CH_4, (e) C_3H_6, and (f) C_3H_8 adsorption isotherms for several typical MOFs at 296 K. C_3H_6 and C_3H_8 adsorption isotherms for **FeMOF-74** are at 318 K, and for **FeMIL-100** are at 303 K.

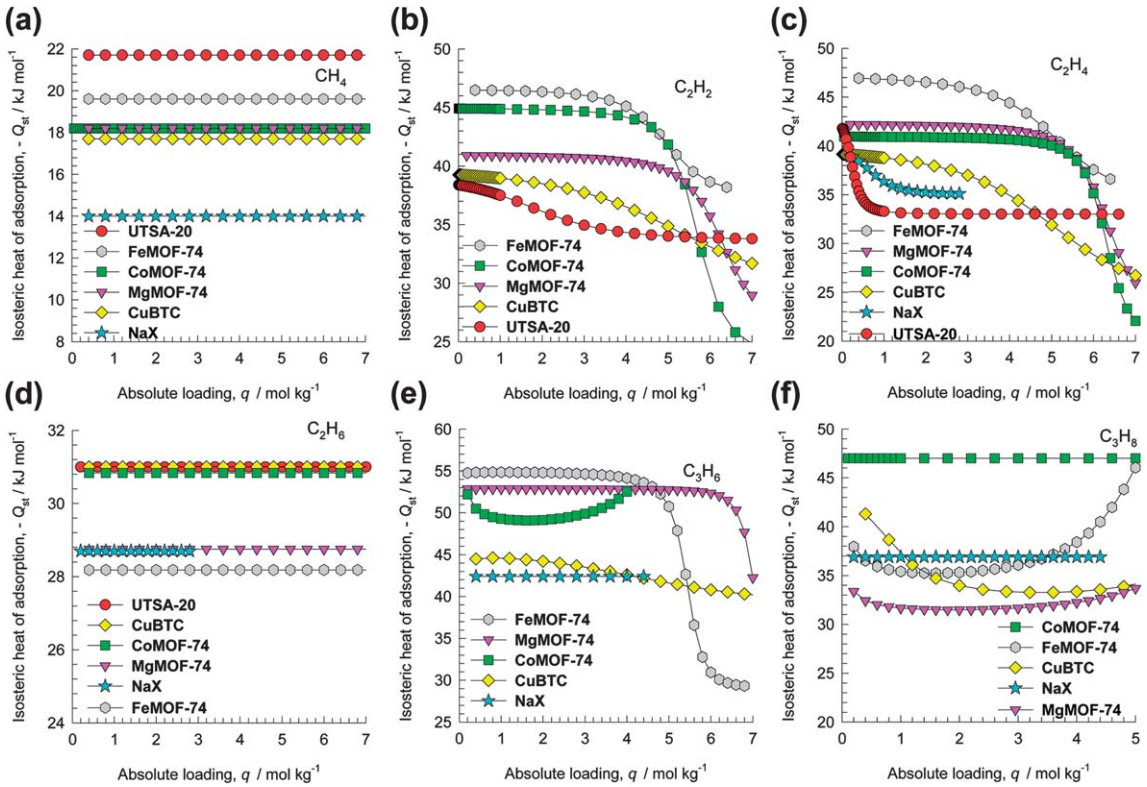

Fig. 2 The isosteric heat of adsorption for (a) CH_4, (b) C_2H_2, (c) C_2H_4, (d) C_2H_6, (e) C_3H_6, and (f) C_3H_8 in selected MOFs. The determination of Q_{st} is based on analytical, or numerical, differentiation of the pure-component isotherm fits using the parameter values provided in the ESI.†

Results and discussions

1. MOF structures investigated for the light hydrocarbon separations

Nineteen different MOFs including the ones with open metal sites (*e.g.* **MgMOF-74**,[62,63] **CoMOF-74**,[64,65] **CuBTC**,[66] **PCN-16**,[67,68] **NOTT-101/102**,[69,70] **UTSA-20**,[71] **MOF-505**,[72] **UMCM-150**[73]) and mixed metal–organic frameworks (M'MOFs[39,40]) were synthesized in our laboratories in order to evaluate their efficacy in each of the above-mentioned separation tasks. Besides the 19 MOFs that we synthesized, the performances of other materials have been evaluated using literature data sources. The ESI† accompanying this publication provides the structural details, synthesis procedures, sorption isotherm data (Fig. S4–24†), and dual-site Langmuir–Freundlich fit parameters (Tables S3–29†). Some of their sorption isotherms for different hydrocarbons are shown in Fig. 1.

Specifically, the performances of various MOFs were evaluated for the following six different *adsorptive* separation tasks.

(1) Separation of CH_4, with 99%+ purity from an equimolar 4-component $CH_4/C_2H_2/C_2H_4/C_2H_6$ mixture.

(2) Investigating the possibility of "fractionating" a 4-component $CH_4/C_2H_2/C_2H_4/C_2H_6$ mixture to obtain each of the constituents in a nearly pure form.

(3) Investigating the possibility of "fractionating" a 6-component $CH_4/C_2H_2/C_2H_4/C_2H_6/C_3H_6/C_3H_8$ mixture to obtain each of the constituents in a nearly pure form.

(4) Separation of an equimolar C_2H_4/C_2H_6 mixture for production of two products: (a) C_2H_4 of 99.5%+ purity (as a feedstock for polymerization), and (b) C_2H_6 of 99%+ purity.

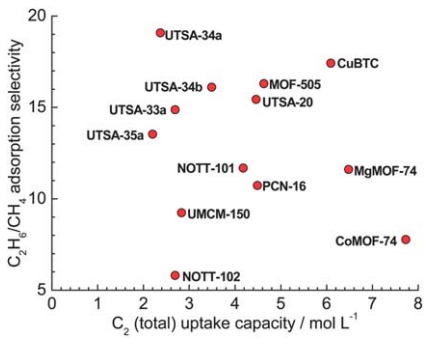

Fig. 3 IAST calculations of the C_2H_6/CH_4 adsorption selectivity *versus* the volumetric uptake capacity of C_2 hydrocarbons (combined total of C_2H_2, C_2H_4, and C_2H_6) for adsorption from an *equimolar* 4-component $CH_4/C_2H_2/C_2H_4/C_2H_6$ mixture at the total bulk gas phase at 296 K and 100 kPa.

(5) Separation of an equimolar C_3H_6/C_3H_8 mixture for production of two products: (a) C_3H_6 of 99.5%+ purity (as a feedstock for polymerization), and (b) C_3H_8 of 99%+ purity.

(6) Selective removal of C_2H_2 from a C_2H_2/C_2H_4 mixture containing 1% C_2H_2 to produce a C_2H_4 product containing <40 ppm C_2H_2.

Separations of these light hydrocarbons are conducted in Pressure Swing Adsorption (PSA) devices. It is well recognized that the separation characteristics of a PSA unit are dictated by a

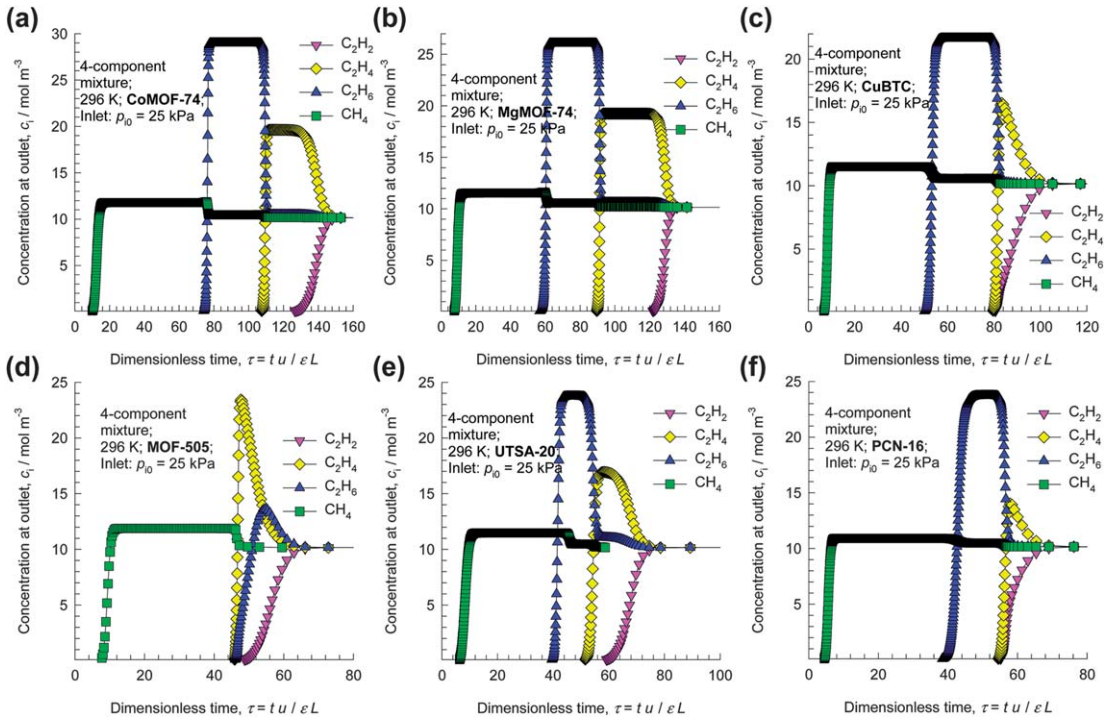

Fig. 4 Breakthrough simulation results for (a) **CoMOF-74**, (b) **MgMOF-74**, (c) **CuBTC**, (d) **MOF-505**, (e) **UTSA-20**, and (f) **PCN-16**, for separation of an *equimolar* 4-component $CH_4/C_2H_2/C_2H_4/C_2H_6$ mixture in a fixed bed of adsorbent at the total bulk gas phase at 296 K and 100 kPa. The *x*-axis represents the dimensionless time, τ.

combination of adsorption selectivity and uptake capacity.[74–76] Generally speaking, higher capacities are desirable because the adsorber bed can be run for a longer length of time before the need for regeneration arises. For a rational choice of adsorbents for mixture separation at high pressures, we need to have a proper method for evaluation that combines the selectivity and capacity metrics in a manner that is a true reflection of the separation performance of a PSA unit. For this purpose, we perform transient breakthrough calculations.[76–78] To demonstrate the fractionation capability of MOFs with open metal sites, we also carry out pulse chromatographic simulations. The breakthrough simulation methodologies, with step- or pulse-inputs of gas mixtures, are provided in the ESI,† along with validations based on comparisons with available literature data.

2. Isosteric heat of adsorption

The binding energies of CH_4, C_2H_2, C_2H_4, C_2H_6, C_3H_6, and C_3H_8 in different MOFs are reflected in the isosteric heat of adsorption, Q_{st}, defined as

$$Q_{st} = RT^2\left(\frac{\partial \ln p}{\partial T}\right)_q \qquad (1)$$

These values were determined using the pure-component isotherm fits. Fig. 2 presents data on the loading dependence of $-Q_{st}$ of six different guest molecules in a small selection of the MOFs, which prove to be promising candidates in this study. The ability of any given structure to separate an alkene–alkane mixture is dependent, *inter alia*, on the differences in the adsorption strengths. A careful examination of the data in Fig. 2 reveals that for MOFs with open metal sites, **CoMOF-74**, **MgMOF-74**, and **FeMOF-74**, the values of $-Q_{st}$ for alkenes are significantly higher than those of the corresponding alkanes with the same number of carbon atoms. For **FeMOF-74**, Bloch *et al.* have established that this is because each alkene molecule attaches *side-on* to an Fe(II) atom within the **FeMOF-74** framework.[43] This large difference in the $-Q_{st}$ values is the prime reason for the superior performance of **MOF-74** in separating alkenes from alkanes as we shall demonstrate later in this article.

3. Evaluation of MOFs for separation of CH_4 from a mixture of C_2 hydrocarbons

Let us first consider the separation of CH_4 from a mixture of C_2 hydrocarbons. Rather than restricting our investigations to just

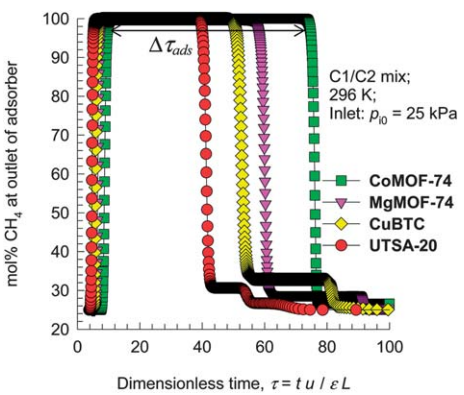

Fig. 5 Mole percentage of CH_4 in the exit gas stream as a function of the dimensionless time, τ, for four typical MOFs.

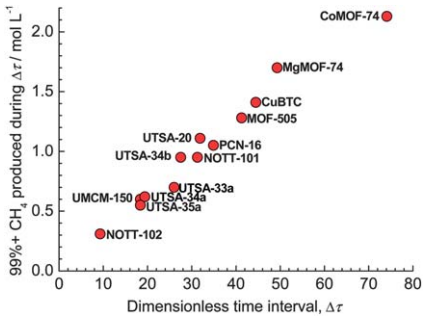

Fig. 6 Plot of 99%+ pure CH_4 produced, per litre of the adsorbent material, during the time interval, $\Delta\tau$, plotted as a function of the time interval, $\Delta\tau$.

binary CH_4/C_2H_6 mixtures, we consider the selective adsorption of C_2 hydrocarbons from an equimolar 4-component $CH_4/C_2H_2/C_2H_4/C_2H_6$ mixture. The choice of such a mixture is dictated by the fact that such mixture separations are encountered in the process of oxidative coupling of methane for producing ethylene. The hierarchy of adsorption strengths is commonly $CH_4 < C_2H_6 < C_2H_4 < C_2H_2$, making the CH_4/C_2H_6 separation the crucial one. This implies that the conclusions drawn about the relative performance of different MOFs will hold equally well for the separation of a binary CH_4/C_2H_6 mixture.

For the purpose of comparing different MOFs, we used two different metrics. The first metric is the *adsorption selectivity*, defined as

$$S_{\text{ads}} = \frac{q_1/q_2}{p_1/p_2} \tag{2}$$

that is determined using the Ideal Adsorbed Solution Theory (IAST) of Myers and Prausnitz.[79] Here p_1 and p_2 are taken to be the partial pressures of C_2H_6 and CH_4, respectively. q_1 and q_2 are the molar loadings in the adsorbed phase of C_2H_6 and CH_4, respectively, expressed in moles per kg of the adsorbent material. The second metric of relevance is the *uptake capacity*. The separation performance of a 4-component $CH_4/C_2H_2/C_2H_4/C_2H_6$ mixture will be dictated by the amount of combined total uptake of C_2 hydrocarbons. Fig. 3 presents IAST calculations of the C_2H_6/CH_4 adsorption selectivity *versus* the uptake capacity of C_2 hydrocarbons (combined total of C_2H_2, C_2H_4, and C_2H_6) for adsorption from an *equimolar* 4-component $CH_4/C_2H_2/C_2H_4/C_2H_6$ mixture at the total bulk gas phase at 296 K and 100 kPa. The uptake capacity is expressed in volumetric terms, *i.e.* as moles per litre of the adsorbent material. We observe from Fig. 3 that **UTSA-34a** has the highest selectivity, but a relatively low uptake capacity. **CoMOF-74** and **MgMOF-74** have the highest uptake capacities. Clearly, selectivity and capacity metrics do not appear to go hand-in-hand.

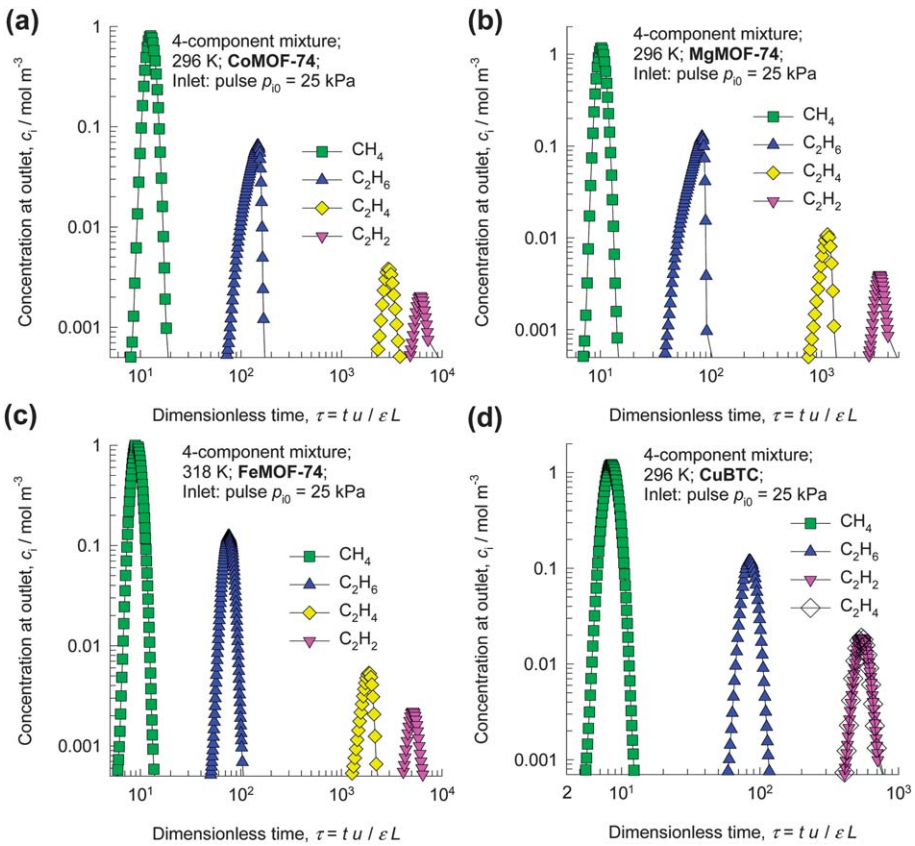

Fig. 7 Pulse chromatographic simulations for separation of an *equimolar* 4-component $CH_4/C_2H_2/C_2H_4/C_2H_6$ mixture with (a) **CoMOF-74**, (b) **MgMOF-74**, (c) **FeMOF-74**, and (d) **CuBTC** as adsorbent materials. For the calculations in (a), (b), and (d), the total bulk gas phase is at 296 K and 100 kPa. In (c), the simulations are performed at 318 K and a total pressure of 100 kPa. A pulse of an *equimolar* 4-component mixture is injected for 10 s at the start of the process, and subsequently the adsorbed components are desorbed by the use of a purge inert gas. It is noteworthy that the areas under each of the peaks are identical for each of the species in the mixture; this aspect is not obvious in view of the log–log nature of the plots.

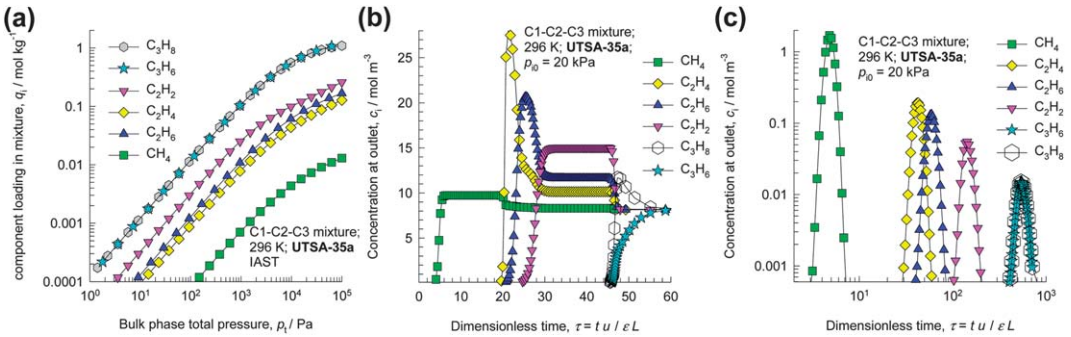

Fig. 8 Separation of an *equimolar* 6-component $CH_4/C_2H_2/C_2H_4/C_2H_6/C_3H_6/C_3H_8$ mixture with **UTSA-35a** at 296 K. (a) IAST calculations of the component loadings in the mixture as a function of the total bulk gas pressure, p_t. (b) Breakthrough simulation results with a step-input of an *equimolar* 6-component mixture into a fixed bed of adsorbent at the total bulk gas phase of 120 kPa. The *x*-axis represents the dimensionless time, τ. (c) Transient breakthrough of a fixed bed of adsorbent to which a pulse-input of an *equimolar* 6-component mixture is injected for 10 s at the start of the process, and subsequently the adsorbed components are desorbed by the use of a purge inert gas. It is noteworthy that the areas under each of the peaks in (c) are identical for each of the species in the mixture; this aspect is not obvious in view of the log–log nature of the plot.

In order to properly evaluate the separation performance of a PSA unit, we performed breakthrough calculations with a step-input of an equimolar 4-component $CH_4/C_2H_2/C_2H_4/C_2H_6$ mixture. Fig. 4 presents data on the concentrations at the exit of the adsorber for six chosen MOFs, for illustration purposes. The *x*-axis in Fig. 4 represents the dimensionless time, τ, defined by dividing the actual time, t, by the characteristic time, $\frac{L\varepsilon}{u}$. All

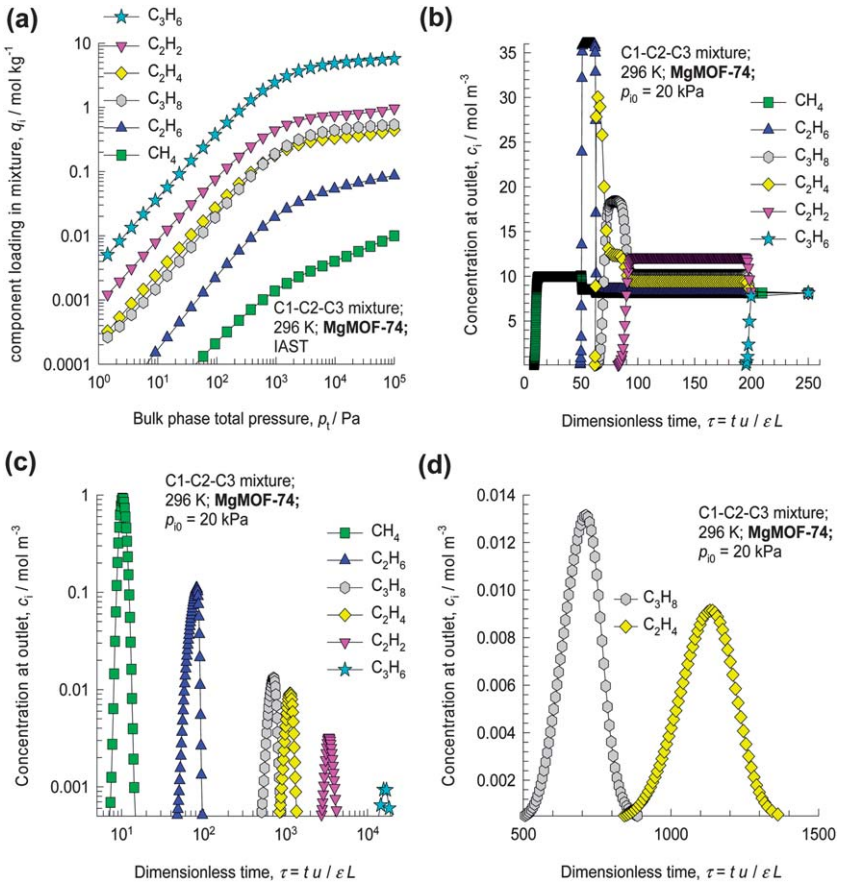

Fig. 9 Separation of an *equimolar* 6-component $CH_4/C_2H_2/C_2H_4/C_2H_6/C_3H_6/C_3H_8$ mixture with **MgMOF-74** at 296 K. (a) IAST calculations of the component loadings in the mixture as a function of the total bulk gas pressure, p_t. (b) Breakthrough simulation results with a step-input of an *equimolar* 6-component mixture into a fixed bed of adsorbent at the total bulk gas phase of 120 kPa. The *x*-axis represents the dimensionless time, τ. (c and d) Transient breakthrough of a fixed bed of adsorbent to which a pulse-input of an *equimolar* 6-component mixture is injected for 10 s at the start of the process, and subsequently the adsorbed components are desorbed by the use of a purge inert gas. It is noteworthy that the areas under each of the peaks in (c) are identical for each of the species in the mixture; this aspect is not obvious in view of the log–log nature of the plot.

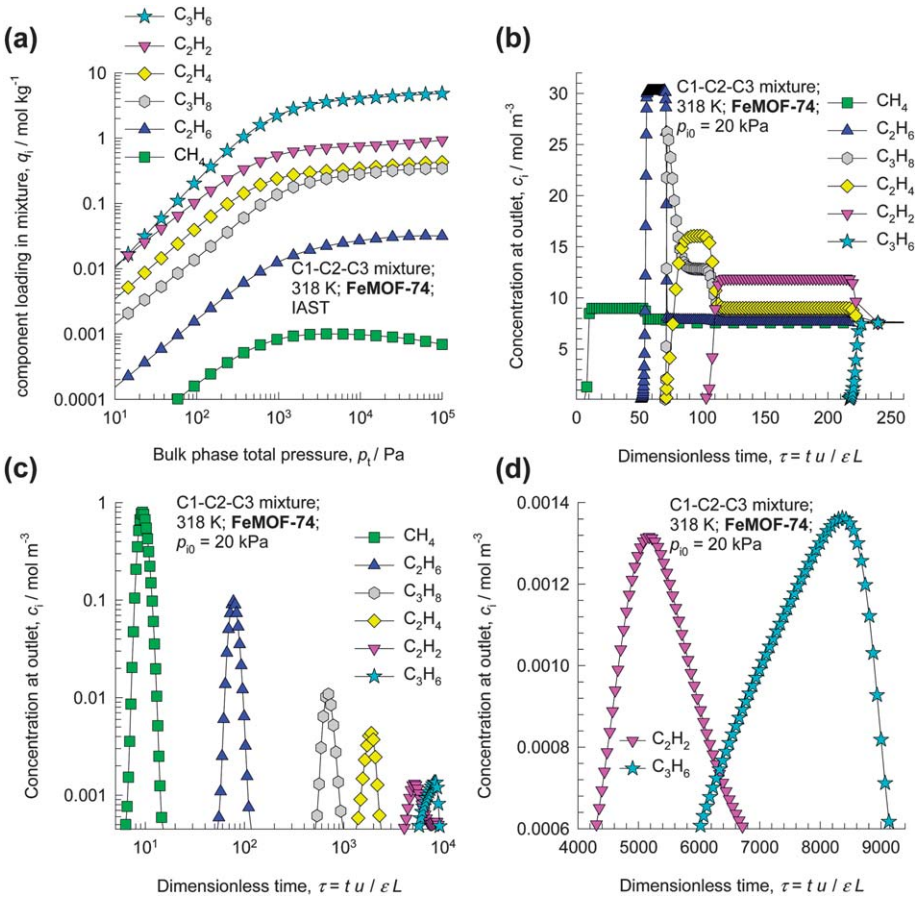

Fig. 10 Separation of an *equimolar* 6-component $CH_4/C_2H_2/C_2H_4/C_2H_6/C_3H_6/C_3H_8$ mixture with **FeMOF-74** at 318 K. (a) IAST calculations of the component loadings in the mixture as a function of the total bulk gas pressure, p_t. (b) Breakthrough simulation results with a step-input of an *equimolar* 6-component mixture into a fixed bed of adsorbent at the total bulk gas phase of 120 kPa. The *x*-axis represents the dimensionless time, τ. (c and d) Transient breakthrough of a fixed bed of adsorbent to which a pulse-input of an *equimolar* 6-component mixture is injected for 10 s at the start of the process, and subsequently the adsorbed components are desorbed by the use of a purge inert gas. It is noteworthy that the areas under each of the peaks in (c) are identical for each of the species in the mixture; this aspect is not obvious in view of the log–log nature of the plot.

adsorbents have the ability of separating CH_4 in a pure form from this quaternary mixture. **CoMOF-74** and **MgMOF-74** are of special interest because the breakthrough characteristics indicate the possibility that each of the individual components in the 4-component mixture can be obtained in its pure form.

From the data presented in Fig. 4, we can determine the mol% CH_4 in the exit gas stream. Fig. 5 shows some typical plots of mol% CH_4 in the exit gas stream as a function of the dimensionless time, τ, for a few typical MOFs. Assuming, arbitrarily, that a purity level of 99%+ CH_4 is desired, we can determine the corresponding dimensionless time interval, $\Delta\tau$. The amount of CH_4, with the chosen 99%+ purity level, can be determined from a material balance over the adsorber by integrating the amount of CH_4 in the outlet gas during the time interval $\Delta\tau$. Each MOF has a different value of $\Delta\tau$ during which 99%+ CH_4 is available. Fig. 5 shows that the value of $\Delta\tau$ is highest for **CoMOF-74**, and it is to be expected that the production capacity of this MOF would also be the highest.

Fig. 6 presents a plot of 99%+ pure CH_4 produced, per litre of the adsorbent material, during the time interval, $\Delta\tau$, plotted as a function of the time interval, $\Delta\tau$. There is a reasonably good correlation between the productivity of CH_4 and $\Delta\tau$; this relationship is practically a linear one. From these results we note that the hierarchy of production capacities, per litre of the adsorbent, is **CoMOF-74 > MgMOF-74 > CuBTC > MOF-505 > UTSA-20**. All other MOFs have significantly lower production capacities and are not viable adsorbents for use in practice. It is remarkable to note that this hierarchy is not dictated by the

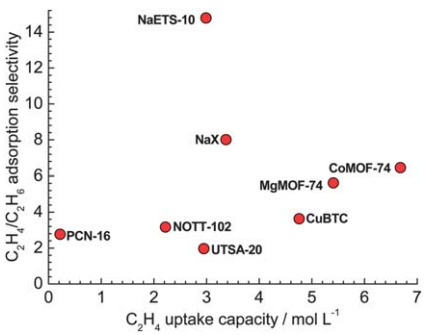

Fig. 11 IAST calculations of the C_2H_4/C_2H_6 adsorption selectivity *versus* the volumetric uptake capacity of C_2H_4 for adsorption from an *equimolar* C_2H_4/C_2H_6 mixture at the total bulk gas phase at 296 K and 100 kPa.

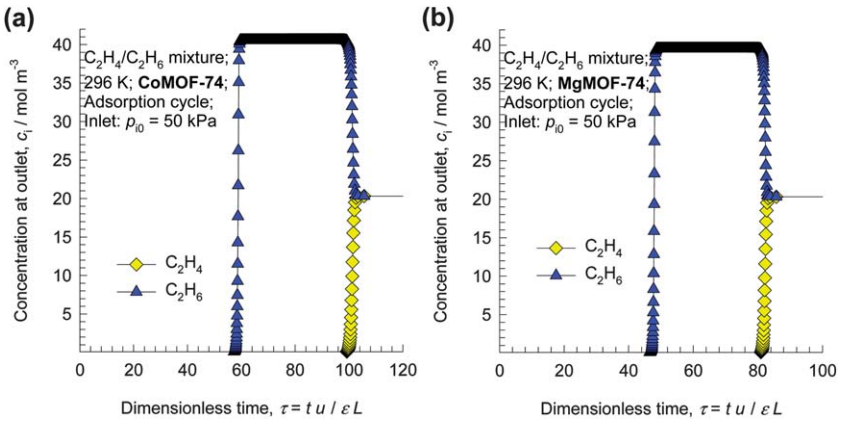

Fig. 12 Transient breakthrough of an *equimolar* ethylene–ethane mixture in an adsorber bed packed with (a) **CoMOF-74** and (b) **MgMOF-74** in the adsorption phase of a PSA operation. The inlet gas is maintained at partial pressures $p_1 = p_2 = 50$ kPa, at a temperature of 296 K.

adsorption selectivity, but by a *combination* of adsorption selectivity and uptake capacity. Uptake capacities are of paramount importance in determining the performance of PSA units, as is evident from the fact that **CoMOF-74** and **MgMOF-74** have the best productivities, despite their only modest adsorption selectivities.

4. Adsorptive "fractionation" of $CH_4/C_2H_2/C_2H_4/C_2H_6$ mixtures

The breakthrough curves shown in Fig. 4 reveal some additional special features of **CoMOF-74** and **MgMOF-74** because the breakthrough times for each component, following the hierarchy $CH_4 < C_2H_6 < C_2H_4 < C_2H_2$, are significantly different from each other. This implies that it may be possible to recover each component in a nearly pure form, which is a most desirable property. In order to further explore this property, we carried out pulse chromatographic simulations for separation of an equimolar 4-component $CH_4/C_2H_2/C_2H_4/C_2H_6$ mixture. Fig. 7 presents the representative results obtained with (a) **CoMOF-74**, (b) **MgMOF-74**, (c) **FeMOF-74**, and (d) **CuBTC**. Of these materials, the breakthrough characteristics of **CoMOF-74**, **MgMOF-74**, and **FeMOF-74** are remarkable. For these three materials, it appears that it is possible to obtain each individual component in its pure form. Such "fractionation" ability is not possessed by any of the other MOFs examined in this study. For example, with **CuBTC**, the peaks of C_2H_2 and C_2H_4 overlap, signifying the fact that separation of C_2H_2/C_2H_4 mixtures is difficult with **CuBTC** as an adsorbent.

5. Adsorptive "fractionation" of $CH_4/C_2H_2/C_2H_4/C_2H_6/C_3H_6/C_3H_8$ mixtures

In the study of He *et al.*,[58] it has been demonstrated that **UTSA-35a** has the potential of separating an equimolar 6-component $CH_4/C_2H_2/C_2H_4/C_2H_6/C_3H_6/C_3H_8$ mixture to obtain individual fractions based on the number of carbon atoms, *i.e.* C_1, C_2, and C_3 fractions. This ability of **UTSA-35a** to obtain individual C_1, C_2, and C_3 fractions is clearly demonstrated by the pulse chromatographic simulations for an equimolar 6-component mixture, see Fig. 8c. **UTSA-35a** is not capable of separating C_3H_6/C_3H_8 mixtures, and the reason for this can be found in the IAST calculations of the component loadings in Fig. 8a. We note that the adsorption loadings of C_3H_6 and C_3H_8 are practically identical in the whole range of pressures. A further implication is that the breakthrough times for C_3H_6 and C_3H_8 in a fixed bed

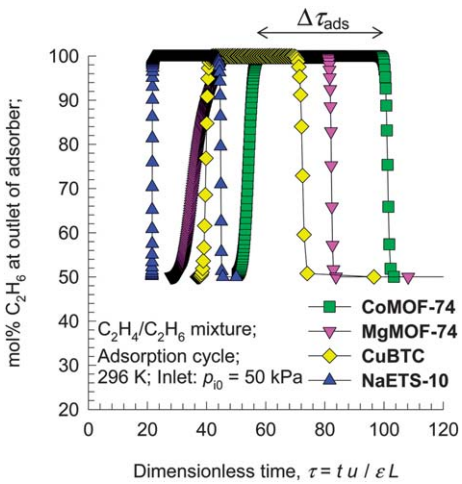

Fig. 13 Mole percentage of C_2H_6 in the outlet gas of an adsorber bed packed with **CoMOF-74**, **MgMOF-74**, **CuBTC**, and **NaETS-10** in the adsorption cycle. The inlet gas is maintained at partial pressures $p_1 = p_2 = 50$ kPa, at a temperature of 296 K.

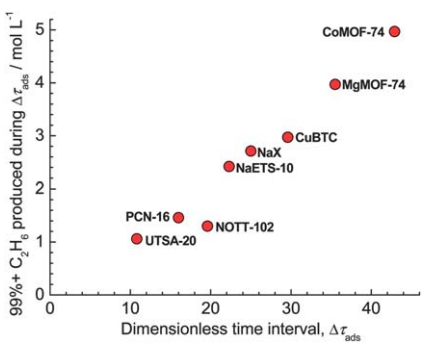

Fig. 14 A plot of 99%+ pure C_2H_6 produced, per litre of adsorbent materials, during the time interval $\Delta\tau_{ads}$, plotted as a function of the time interval, $\Delta\tau_{ads}$.

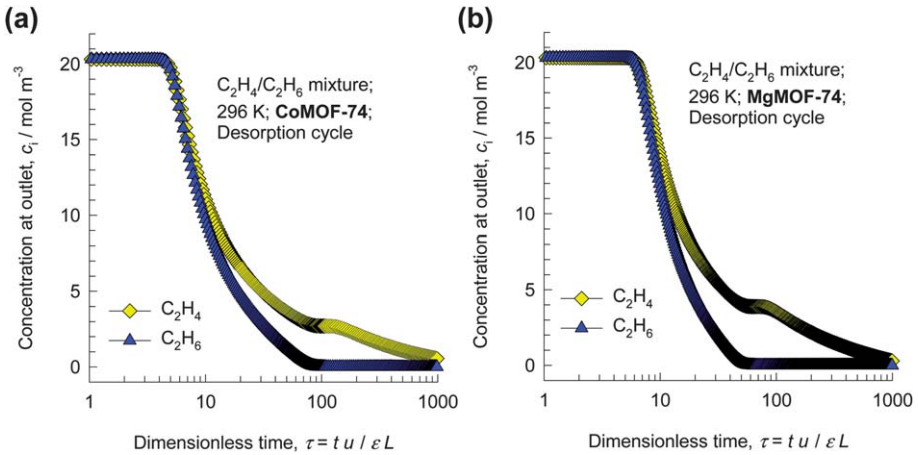

Fig. 15 Transient breakthrough of an *equimolar* ethylene–ethane mixture in an adsorber bed packed with (a) **CoMOF-74** and (b) **MgMOF-74** in the desorption cycle of a PSA operation. The contents of the bed, which is equilibrated at partial pressures $p_1 = p_2 = 50$ kPa, at a temperature of 296 K, are subjected to purging by an inert gas.

adsorber are practically identical, see Fig. 8b. The IAST calculations also show that the component loadings of C_2H_4 and C_2H_6 are close to each other. Consequently, the peaks of C_2H_4 and C_2H_6 in the pulse simulations tend to overlap, see Fig. 8c.

MgMOF-74 and **FeMOF-74** are much more potent. These two MOFs are capable of separating the 6-component mixture to obtain each of the components in a nearly pure form. The supporting data are presented in Fig. 9 and 10. These figures provide (a) IAST calculations, (b) breakthroughs in a fixed bed adsorber with step-inputs, and (c and d) pulse chromatographic simulations (two different scales are used in (c) and (d) for the same set of results to more clearly show the fractionation capabilities). The sequence of breakthroughs of the pulses in (c) and (d) of each component that emerge is dictated by the hierarchy in the component loadings in the IAST calculations.

According to our calculations (not shown here), **CoMOF-74** has similar fractionation capability as **MgMOF-74** and **FeMOF-74**. The US patent awarded to Matzger *et al.*[56] presents pulse breakthrough experimental curves for separation of C_2H_4/C_2H_6 and C_3H_6/C_3H_8 mixtures in fixed beds packed with **CoMOF-74**. These curves clearly demonstrate the fractionation capability of both binary mixtures. In the ESI,† pulse chromatographic simulation results for these mixtures are presented in order to demonstrate the agreement, albeit qualitatively, with the experimental results quoted in the patent.

6. Evaluation of MOFs for separation of C_2H_4/C_2H_6 mixtures

Let us consider the separation of binary C_2H_4/C_2H_6 mixtures using MOFs that have a reasonable separation selectivity based on the information already obtained in the foregoing analysis of the different MOF structures. Separation of C_2H_4/C_2H_6 mixtures is industrially important in the context of production of polymer-grade ethylene, whose purity needs to be 99.5%+. Furthermore, for comparison purposes, the performances of **NaX zeolite**[59] and **NaETS-10**[61] were also evaluated. Fig. 11 shows the IAST calculations of the C_2H_4/C_2H_6 adsorption selectivity *versus* the volumetric uptake capacity of C_2H_4 for adsorption from an equimolar C_2H_4/C_2H_6 mixture at the total bulk gas phase at

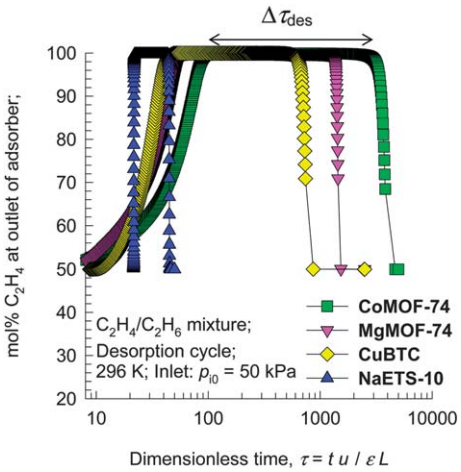

Fig. 16 Mole percentage of C_2H_4 in the outlet gas of an adsorber bed packed with **CoMOF-74**, **MgMOF-74**, **CuBTC**, and **NaETS-10** in the desorption cycle. The contents of the bed, which is equilibrated at partial pressures $p_1 = p_2 = 50$ kPa, at a temperature of 296 K, are subjected to purging by an inert gas.

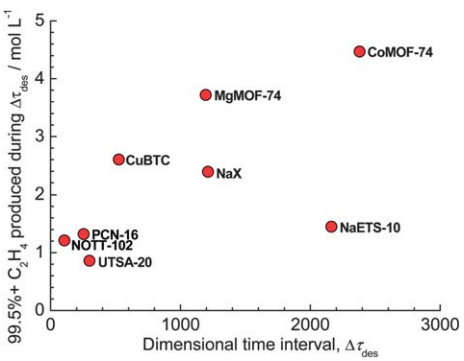

Fig. 17 A plot of 99.5%+ pure C_2H_4 produced, per litre of adsorbents, during the time interval, $\Delta\tau_{des}$, as a function of the time interval, $\Delta\tau_{des}$.

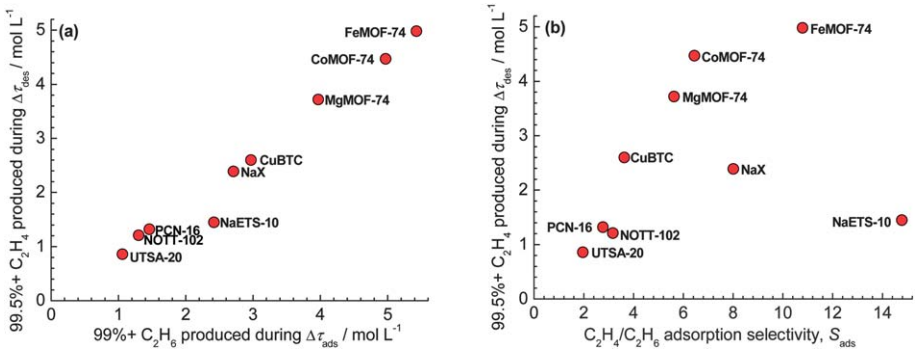

Fig. 18 A comparison of various MOFs for productivity of 99.5%+ pure C_2H_4 expressed as a function of (a) productivity of 99%+ pure C_2H_6 and (b) C_2H_4/C_2H_6 adsorption selectivity. The conditions chosen are: $p_1 = p_2 = 50$ kPa, and $T = 296$ K. The data for **FeMOF-74** are at 318 K, and therefore considered to be conservative.

296 K and 100 kPa. The highest selectivity is obtained with **NaETS-10**, a material patented by Engelhard, but this material has only a limited uptake capacity. **CoMOF-74** and **MgMOF-74** have uptake capacities that are about twice as high as that for **NaETS-10**, albeit with lower selectivities.

For separations in a PSA adsorption device, we need to produce each of the two components in the mixture in a nearly pure form. The process occurs in two cycles. Let us first consider the adsorption cycle, in which C_2H_4 is selectively adsorbed. Fig. 12 shows transient breakthrough of an equimolar ethylene–ethane mixture in an adsorber bed packed with (a) **CoMOF-74** and (b) **MgMOF-74**, chosen to illustrate just two of the several MOFs investigated. The inlet gas is maintained at partial pressures $p_1 = p_2 = 50$ kPa, at a temperature of 296 K. From the gas phase concentrations at the exit of the adsorber, we can determine the mol% C_2H_6. This information is presented in Fig. 13. Let us arbitrarily choose the required purity of C_2H_6 to be 99%+. From Fig. 13, we can determine the time interval $\Delta\tau_{ads}$ for each of the MOFs during which the purity level of C_2H_6 is 99%+. A material balance on the adsorber, obtained by integrating the amount of 99%+ pure C_2H_6 collected at the exit during this time interval $\Delta\tau_{ads}$, can be determined for each of the MOFs. Fig. 14 presents a plot of 99%+ pure C_2H_6 produced, per litre of the adsorbent material, during the time interval $\Delta\tau_{ads}$, plotted as a function of the time interval, $\Delta\tau_{ads}$. There is a nearly perfect linear relation between the production of 99%+ pure C_2H_6 and the time interval $\Delta\tau_{ads}$. From these results, we note that the hierarchy of C_2H_6 production capacities, per litre of the adsorbent, is **CoMOF-74 > MgMOF-74 > CuBTC > NaX > NaETS-10 > PCN-16 > NOTT-102 > UTSA-20**. The high productivities of **CoMOF-74** and **MgMOF-74** can be traced to the high uptake capacities.

Once the entire bed is in equilibrium with the partial pressures $p_1 = p_2 = 50$ kPa, at a temperature of 296 K, the desorption cycle is initiated, say with a purge (inert) gas. Fig. 15 illustrates transient breakthrough of an equimolar ethylene–ethane mixture in an adsorber bed packed with (a) **CoMOF-74** and (b) **MgMOF-74** in the desorption cycle of a PSA operation. During the desorption cycle, nearly pure C_2H_4 can be recovered. Fig. 16 shows mol % C_2H_4 in the outlet gas of an adsorber bed packed using three representative MOFs (**CoMOF-74**, **MgMOF-74**, and **CuBTC**) and **NaETS-10** in the desorption cycle. For production of ethylene as a feedstock for polymerization purposes, the required purity level is 99.5%+. From Fig. 16, we can determine the time interval, $\Delta\tau_{des}$, for each of the MOFs, during which the purity level of C_2H_4 is 99.5%+. A material balance on the adsorber, obtained by integrating the amount of 99.5%+ pure C_2H_4 collected at the exit during this time interval, $\Delta\tau_{des}$, can be determined for each of the MOFs. Fig. 17 presents a plot of 99.5%+ pure C_2H_4 produced, per litre of the adsorbent, during

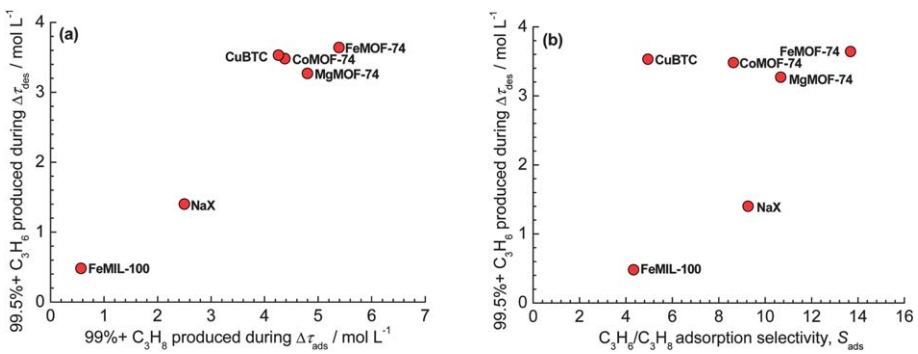

Fig. 19 A comparison of various MOFs for productivity of 99.5%+ pure C_3H_6 expressed as a function of (a) productivity of 99%+ pure C_3H_8, and (b) C_3H_6/C_3H_8 adsorption selectivity. The conditions chosen are: $p_1 = p_2 = 10$ kPa and $T = 296$ K. The choice of the partial pressures is dictated by the fact that the isotherms for **FeMIL-100** are only available with a pressure of 20 kPa. The data for **FeMOF-74** are at 318 K, and therefore considered to be conservative. The data for **FeMIL-100** are at 303 K.

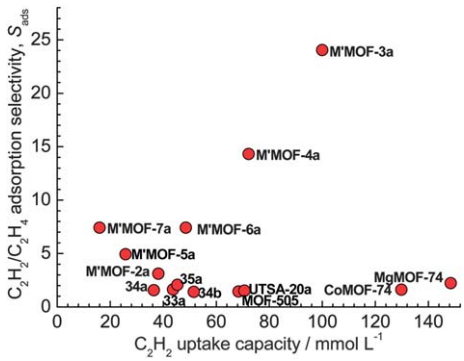

Fig. 20 IAST calculations of the C_2H_2/C_2H_4 adsorption selectivity *versus* the volumetric uptake capacity of C_2H_2 for adsorption from C_2H_2/C_2H_4 mixtures containing 1% C_2H_2. The partial pressures of C_2H_2 and C_2H_4 are $p_1 = 1$ kPa and $p_2 = 99$ kPa, respectively.

the time interval, $\Delta\tau_{des}$, plotted as a function of the time interval, $\Delta\tau_{des}$. From these results we note that the hierarchy of C_2H_4 production capacities, per litre of the adsorbent, is **CoMOF-74 > MgMOF-74 > CuBTC > NaX > NaETS-10 > PCN-16 > NOTT-102 > UTSA-20**. The good productivity of **CoMOF-74** and **MgMOF-74** can be traced to the high uptake capacities. On the other hand, we note that the high selectivity of **NaETS-10** for C_2H_4/C_2H_6 separation does not ensure its good productivity in the PSA adsorber because of its limited capacity.

The results presented in Fig. 14 and 17 can be combined to summarize the data on productivities of 99%+ pure C_2H_6 and 99.5%+ pure C_2H_4 by plotting the productivities against each other. For separation at a total pressure of 100 kPa and a temperature of 296 K, the data are summarized in the cross-plot presented in Fig. 18a; also included here are calculations for **FeMOF-74** for which data are available at 318 K. **FeMOF-74**, **CoMOF-74** and **MgMOF-74** clearly are the leading contenders for separation of C_2H_4/C_2H_6 mixtures. Fig. 18b presents a plot of the productivity of various MOFs for ethylene, expressed as a function of S_{ads}. We note that **NaETS-10**, with the highest value of S_{ads}, has a productivity that is only about a third of **FeMOF-74**, **CoMOF-74** and **MgMOF-74**.

7. Evaluation of MOFs for separation of C_3H_6/C_3H_8 mixtures

Let us consider the separation of binary C_3H_6/C_3H_8 mixtures that is of importance in the context of production of polymer-grade propylene, whose purity needs to be 99.5%+. For comparison purposes, the performances of **NaX zeolite**[60] and **FeMIL-100**[46] were also evaluated. The calculation procedure is exactly analogous to that presented in the earlier section for ethylene–ethane mixtures. The final comparison results for the productivities of 99.5%+ pure C_3H_6 are presented in Fig. 19. **FeMOF-74**, **CoMOF-74**, and **MgMOF-74** have significantly higher productivities than other materials such as **NaX**,[60] and **FeMIL-100**[46] that have been suggested in the literature for this propylene production.

8. Evaluation of MOFs for separation of C_2H_2/C_2H_4 mixtures

In steam cracking of ethane to produce ethylene, one of the byproducts is ethyne. Ethyne has a deleterious effect on end-products of ethylene, such as polyethylene. Therefore, recovery or removal of ethyne from ethylene streams is essential because the presence of ethyne at levels higher than 40 ppm will poison the catalyst. The selective removal of ethyne is conventionally carried out by absorption in DMF, which is energy-intensive. Selective adsorption is an energy-efficient alternative.

Let us consider the separation of a binary C_2H_2/C_2H_4 mixture containing 1%, *i.e.* 10 000 ppm, of C_2H_2 in the mixture. Fig. 20 presents the IAST calculations of the C_2H_2/C_2H_4 adsorption selectivity *versus* the volumetric uptake capacity of C_2H_2 for adsorption from C_2H_2/C_2H_4 mixtures containing 1% C_2H_2. The highest adsorption selectivity is with **M'MOF-3a**, but its capacity for adsorption of C_2H_2 is significantly lower than that of **MgMOF-74** and **CoMOF-74**.

We now compare the separation characteristics of different MOFs for producing C_2H_4 containing less than 40 ppm C_2H_2. As an illustration, Fig. 21 presents the transient breakthrough of a C_2H_2/C_2H_4 feed mixture containing 1% C_2H_2 in an adsorber bed packed with (a) **MgMOF-74** and (b) **CoMOF-74**. From the concentrations at the outlet of the adsorber, we can determine the purity of C_2H_4 in the exit gas stream. Fig. 22 presents a plot

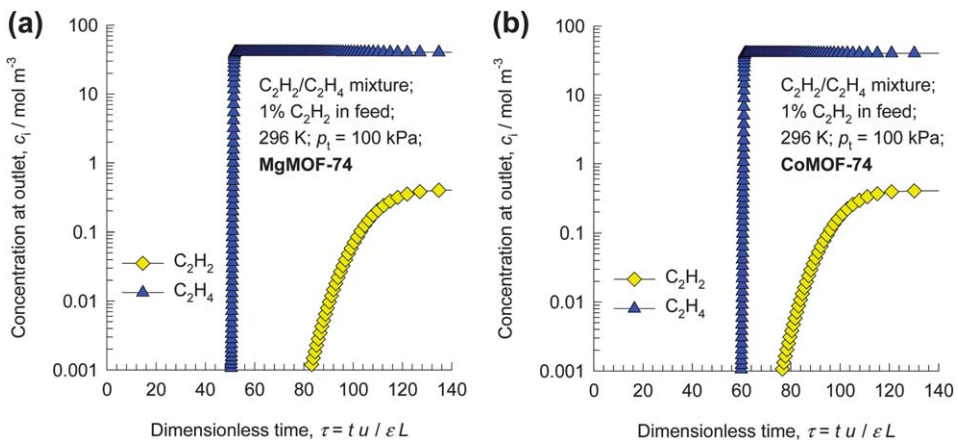

Fig. 21 Transient breakthroughs of a C_2H_2/C_2H_4 mixture containing 1% C_2H_2 mixture in an adsorber bed packed with (a) **MgMOF-74** and (b) **CoMOF-74**. The total bulk gas phase is at 296 K and 100 kPa. The partial pressures of C_2H_2 and C_2H_4 in the inlet feed gas mixture are $p_1 = 1$ kPa and $p_2 = 99$ kPa, respectively.

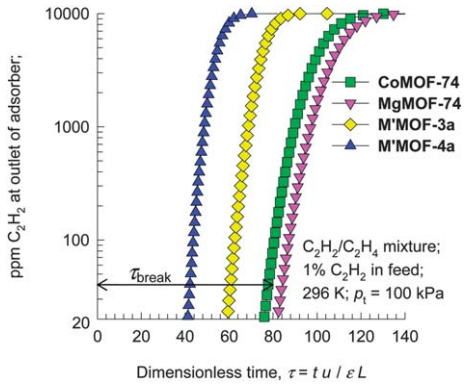

Fig. 22 ppm C_2H_2 in the outlet gas of an adsorber bed packed with **MgMOF-74**, **CoMOF-74**, **M'MOF-3a**, and **M'MOF-4a**. The total bulk gas phase is at 296 K and 100 kPa. The partial pressures of C_2H_2 and C_2H_4 in the inlet feed gas mixture are $p_1 = 1$ kPa and $p_2 = 99$ kPa, respectively.

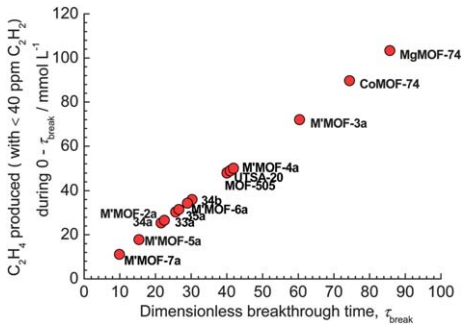

Fig. 23 A plot of C_2H_4 produced, containing less than 40 ppm of C_2H_2, per litre of the adsorbent, during the time interval 0–τ_{break}, plotted as a function of the time, τ_{break}. The breakthrough time, τ_{break}, corresponds to the exit gas containing 40 ppm C_2H_2.

of the ppm C_2H_2 in the outlet gas of an adsorber bed packed with **MgMOF-74**, **CoMOF-74**, **M'MOF-3a**, and **M'MOF-4a**. The breakthrough times, τ_{break}, corresponding to the exit gas containing 40 ppm C_2H_2, can be determined. From a material balance on the adsorber, the production of C_2H_4, with the specified purity level, can be determined by integrating during the time interval 0–τ_{break}. Fig. 23 presents a plot of the amount of C_2H_4 produced, containing less than 40 ppm of C_2H_2, per litre of the adsorbent, during the time interval 0–τ_{break}, plotted as a function of the time, τ_{break}. The hierarchy of production capacities is **MgMOF-74 > CoMOF-74 > M'MOF-3a > M'MOF-4a**. The superior performance of **MgMOF-74** and **CoMOF-74** can be traced to their high capacities to adsorb C_2H_2. **M'MOF-3a** and **M'MOF-4a** have high selectivities but are subject to capacity limitations.

Conclusions

Our study clearly demonstrates that microporous metal–organic frameworks are very promising materials for separations of light hydrocarbons. The separation capacities are dependent on both the selectivities and hydrocarbon uptakes of the microporous MOFs. Although tuning the pore sizes, curvatures, and porosities, to a certain extent, can adjust their separation capacities, the open metal sites still play the most important roles to differentiate their interactions with these light hydrocarbons. Exploration of new microporous MOFs with high density of open metal sites will be highly in need in the near future for the efficient separation of light hydrocarbons. More specifically, the following major conclusions can be drawn from this study.

(1) For separation of CH_4, with 99%+ purity, from an equimolar $CH_4/C_2H_2/C_2H_4/C_2H_6$ mixture, the best materials are **CoMOF-74** and **MgMOF-74**.

(2) **FeMOF-74**, **CoMOF-74**, and **MgMOF-74** are the best MOFs for separation of an equimolar C_2H_4/C_2H_6 mixture for production of two products: (a) C_2H_4 of 99.5%+ purity (as a feedstock for polymerization), and (b) C_2H_6 of 99%+ purity.

(3) **FeMOF-74**, **CoMOF-74**, and **MgMOF-74** are the best MOFs for separation of an equimolar C_3H_6/C_3H_8 mixture for production of two products: (a) C_3H_6 of 99.5%+ purity (as a feedstock for polymerization), and (b) C_3H_8 of 99%+ purity.

(4) **MgMOF-74**, **Co-MOF74**, and **M'MOF-3a** are the three best materials for selective removal of C_2H_2 from a C_2H_2/C_2H_4 mixture containing 10 000 ppm C_2H_2 to produce a C_2H_4 product containing less than 40 ppm C_2H_2.

(5) **MgMOF-74**, **FeMOF-74**, and **CoMOF-74** possess the ability of "fractionating" an equimolar 4-component $CH_4/C_2H_2/C_2H_4/C_2H_6$ mixture to obtain each of the constituents in a nearly pure form, and

(6) **MgMOF-74**, **FeMOF-74**, and **CoMOF-74** possess the ability of "fractionating" an equimolar 6-component $CH_4/C_2H_2/C_2H_4/C_2H_6/C_3H_6/C_3H_8$ mixture to obtain each of the constituents in a nearly pure form.

The overall conclusion that can be drawn from our study is that **FeMOF-74**, **CoMOF-74**, and **MgMOF-74** with high density of open metal sites are versatile adsorbents that can be used in all of the above-mentioned separation tasks, offering high production capacities per litre of adsorbent materials used in a PSA unit.

Abbreviations

Notation

L	Length of the packed bed adsorber, m
n	Number of species in the mixture, dimensionless
p_i	Partial pressure of species i in the mixture, Pa
p_t	Total system pressure, Pa
q_i	Component molar loading of species i, mol kg^{-1}
q_t	Total molar loading in the mixture, mol kg^{-1}
Q_{st}	Isosteric heat of adsorption, kJ mol^{-1}
R	Gas constant, 8.314 J mol^{-1} K^{-1}
S_{ads}	Adsorption selectivity, dimensionless
t	Time, s
T	Absolute temperature, K
u	Superficial gas velocity in the packed bed, m s^{-1}
z	Distance along the adsorber, m.

Greek letters

ε	Voidage of the packed bed, dimensionless
τ	Time, dimensionless
τ_{break}	Breakthrough time, dimensionless.

Subscripts

i	Referring to component i
t	Referring to total mixture.

Acknowledgements

This work was supported by an Award AX-1730 from Welch Foundation (BC).

References

1 J.-R. Li, J. Sculley and H.-C. Zhou, *Chem. Rev.*, 2012, **112**, 869–932.
2 K. Sumida, D. L. Rogow, J. A. Mason, T. M. McDonald, E. D. Bloch, Z. R. Herm, T.-H. Bae and J. R. Long, *Chem. Rev.*, 2012, **112**, 724–781.
3 H. Wu, Q. Gong, D. H. Olson and J. Li, *Chem. Rev.*, 2012, **112**, 836–868.
4 Y.-S. Bae and R. Q. Snurr, *Angew. Chem., Int. Ed.*, 2011, **50**, 11586–11596.
5 H.-L. Jiang and Q. Xu, *Chem. Commun.*, 2011, **47**, 3351–3370.
6 Z. Zhang, S. Xiang and B. Chen, *CrystEngComm*, 2011, **13**, 5983–5992.
7 B. Chen, S. Xiang and G. Qian, *Acc. Chem. Res.*, 2010, **43**, 1115–1124.
8 J.-R. Li, R. J. Kuppler and H.-C. Zhou, *Chem. Soc. Rev.*, 2009, **38**, 1477–1504.
9 S. Horike, S. Shimomura and S. Kitagawa, *Nat. Chem.*, 2009, **1**, 695–704.
10 S. Kitagawa, R. Kitaura and S.-i. Noro, *Angew. Chem., Int. Ed.*, 2004, **43**, 2334–2375.
11 Q. Lin, T. Wu, S.-T. Zheng, X. Bu and P. Feng, *J. Am. Chem. Soc.*, 2012, **134**, 784–787.
12 B. Li, Z. Zhang, Y. Li, K. Yao, Y. Zhu, Z. Deng, F. Yang, X. Zhou, G. Li, H. Wu, N. Nijem, Y. J. Chabal, Z. Lai, Y. Han, Z. Shi, S. Feng and J. Li, *Angew. Chem., Int. Ed.*, 2011, **51**, 1412–1415.
13 Y.-X. Tan, Y.-P. He and J. Zhang, *Chem. Commun.*, 2011, **47**, 10647–10649.
14 T. Panda, P. Pachfule, Y. Chen, J. Jiang and R. Banerjee, *Chem. Commun.*, 2011, **47**, 2011–2013.
15 R. Vaidhyanathan, S. S. Iremonger, G. K. H. Shimizu, P. G. Boyd, S. Alavi and T. K. Woo, *Science*, 2010, **330**, 650–653.
16 J. An, S. J. Geib and N. L. Rosi, *J. Am. Chem. Soc.*, 2010, **132**, 38–39.
17 T. Fukushima, S. Horike, Y. Inubushi, K. Nakagawa, Y. Kubota, M. Takata and S. Kitagawa, *Angew. Chem., Int. Ed.*, 2010, **49**, 4820–4824.
18 E. Q. Procopio, F. Linares, C. Montoro, V. Colombo, A. Maspero, E. Barea and J. A. R. Navarro, *Angew. Chem., Int. Ed.*, 2010, **49**, 7308–7311.
19 J.-P. Zhang and X.-M. Chen, *J. Am. Chem. Soc.*, 2009, **131**, 5516–5521.
20 R. Vaidhyanathan, S. S. Iremonger, K. W. Dawson and G. K. H. Shimizu, *Chem. Commun.*, 2009, 5230–5232.
21 Y.-S. Bae, O. K. Farha, A. M. Spokoyny, C. A. Mirkin, J. T. Hupp and R. Q. Snurr, *Chem. Commun.*, 2008, 4135–4137.
22 M. Hartmann, S. Kunz, D. Himsl and O. Tangermann, *Langmuir*, 2008, **24**, 8634–8642.
23 P. L. Llewellyn, S. Bourrelly, C. Serre, Y. Filinchuk and G. Férey, *Angew. Chem., Int. Ed.*, 2006, **45**, 7751–7754.
24 D. Britt, H. Furukawa, B. Wang, T. G. Glover and O. M. Yaghi, *Proc. Natl. Acad. Sci. U. S. A.*, 2009, **106**, 20637–20640.
25 S. Horike, Y. Inubushi, T. Hori, T. Fukushima and S. Kitagawa, *Chem. Sci.*, 2012, **3**, 116–120.
26 Z.-Y. Gu, C.-X. Yang, N. Chang and X.-P. Yan, *Acc. Chem. Res.*, 2012, **45**, 734–745.
27 B. Chen, C. Liang, J. Yang, D. S. Contreras, Y. L. Clancy, E. B. Lobkovsky, O. M. Yaghi and S. Dai, *Angew. Chem., Int. Ed.*, 2006, **45**, 1390–1393.
28 F. Vermoortele, M. Maes, P. Z. Moghadam, M. J. Lennox, F. Ragon, M. Boulhout, S. Biswas, K. G. M. Laurier, I. Beurroies, R. Denoyel, M. Roeffaers, N. Stock, T. Düren, C. Serre and D. E. D. Vos, *J. Am. Chem. Soc.*, 2011, **133**, 18526–18529.
29 V. Finsy, H. Verelst, L. Alaerts, D. D. Vos, P. A. Jacobs, G. V. Baron and J. F. M. Denayer, *J. Am. Chem. Soc.*, 2008, **130**, 7110–7118.
30 P. S. Bárcia, D. Guimarães, P. A. P. Mendes, J. A. C. Silva, V. Guillerm, H. Chevreau, C. Serre and A. E. Rodrigues, *Microporous Mesoporous Mater.*, 2011, **139**, 67–73.
31 M. A. Moreira, J. C. Santos, A. F. P. Ferreira, U. Müller, N. Trukhan, J. M. Loureiro and A. E. Rodrigues, *Sep. Sci. Technol.*, 2011, **46**, 1995–2003.
32 R. Krishna and J. M. van Baten, *Phys. Chem. Chem. Phys.*, 2011, **13**, 10593–10616.
33 P. S. Bárcia, F. Zapata, J. A. C. Silva, A. E. Rodrigues and B. Chen, *J. Phys. Chem. B*, 2007, **111**, 6101–6103.
34 L. Pan, D. H. Olson, L. R. Ciemnolonski, R. Heddy and J. Li, *Angew. Chem., Int. Ed.*, 2006, **45**, 616–619.
35 Y. He, Z. Zhang, S. Xiang, H. Wu, F. R. Fronczek, W. Zhou, R. Krishna, M. O'Keeffe and B. Chen, *Chem.–Eur. J.*, 2012, **18**, 1901–1904.
36 Y. He, Z. Zhang, S. Xiang, F. R. Fronczek, R. Krishna and B. Chen, *Chem.–Eur. J.*, 2012, **18**, 613–619.
37 M. C. Das, H. Xu, S. Xiang, Z. Zhang, H. D. Arman, G. Qian and B. Chen, *Chem.–Eur. J.*, 2011, **17**, 7817–7822.
38 S. C. Reyes, J. G. Santiesteban, Z. Ni, C. S. Paur, P. Kortunov, J. Zengel and H. W. Deckman, *U.S. Pat.*, US 2009/0216059 A1, 2009.
39 S. Xiang, Z. Zhang, C.-G. Zhao, K. Hong, X. Zhao, D.-L. Ding, M.-H. Xie, C.-D. Wu, R. Gill, K. M. Thomas and B. Chen, *Nat. Commun.*, 2011, **2**, 204.
40 M. C. Das, Q. Guo, Y. He, J. Kim, C.-G. Zhao, K. Hong, S. Xiang, Z. Zhang, K. M. Thomas, R. Krishna and B. Chen, *J. Am. Chem. Soc.*, 2012, **134**, 8703–8710.
41 C. Gücüyener, J. v. d. Bergh and J. Gascon, *J. Am. Chem. Soc.*, 2010, **132**, 17704–17706.
42 J. V. D. Bergh, C. Gücüyener, E. A. Pidko, E. J. M. Hensen, J. Gascon and F. Kapteijn, *Chem.–Eur. J.*, 2011, **17**, 8832–8840.
43 E. D. Bloch, W. L. Queen, R. Krishna, J. M. Zadrozny, C. M. Brown and J. R. Long, *Science*, 2012, **335**, 1606–1610.
44 Y.-S. Bae, C. Y. Lee, K. C. Kim, O. K. Farha, P. Nickias, J. T. Hupp, S. T. Nguyen and R. Q. Snurr, *Angew. Chem., Int. Ed.*, 2012, **51**, 1857–1860.
45 Z. Bao, S. Alnemrat, L. Yu, I. Vasiliev, Q. Ren, X. Lu and S. Deng, *Langmuir*, 2011, **27**, 13554–13562.
46 J. W. Yoon, Y.-K. Seo, Y. K. Hwang, J.-S. Chang, H. Leclerc, S. Wuttke, P. Bazin, A. Vimont, M. Daturi, E. Bloch, P. L. Llewellyn, C. Serre, P. Horcajada, J.-M. Grenèche, A. E. Rodrigues and G. Férey, *Angew. Chem., Int. Ed.*, 2010, **49**, 5949–5952.
47 J. W. Yoon, I. T. Jang, K.-Y. Lee, Y. K. Hwang and J.-S. Chang, *Bull. Korean Chem. Soc.*, 2010, **31**, 220–223.
48 C. Y. Lee, Y.-S. Bae, N. C. Jeong, O. K. Farha, A. A. Sarjeant, C. L. Stern, P. Nickias, R. Q. Snurr, J. T. Hupp and S. T. Nguyen, *J. Am. Chem. Soc.*, 2011, **133**, 5228–5231.
49 K. Li, D. H. Olson, J. Seidel, T. J. Emge, H. Gong, H. Zeng and J. Li, *J. Am. Chem. Soc.*, 2009, **131**, 10368–10369.
50 S. Uchida, R. Eguchi, S. Nakamura, Y. Ogasawara, N. Kurosawa and N. Mizuno, *Chem. Mater.*, 2012, **24**, 325–330.
51 S. Uchida, R. Kawamoto, H. Tagami, Y. Nakagawa and N. Mizuno, *J. Am. Chem. Soc.*, 2008, **130**, 12370–12376.
52 A. F. P. Ferreira, J. C. Santos, M. G. Plaza, N. Lamia, J. M. Loureiro and A. E. Rodrigues, *Chem. Eng. J.*, 2011, **167**, 1–12.
53 A. Wagener, M. Schindler, F. Rudolphi and S. Ernst, *Chem. Ing. Tech.*, 2007, **79**, 851–855.
54 M. G. Plaza, A. M. Ribeiro, A. Ferreira, J. C. Santos, U.-H. Lee, J.-S. Chang, J. M. Loureiro and A. E. Rodrigues, *Sep. Purif. Technol.*, 2012, **90**, 109–119.

55 H. Bux, C. Chmelik, R. Krishna and J. Caro, *J. Membr. Sci.*, 2011, **369**, 284–289.
56 A. J. Matzger, A. G. Wong-Foy and S. Caskey, *U.S. Pat.*, US 2010/0258004 A1, 2010.
57 C. Serre, A. Vimont, P. Llewllyn, J.-S. Chang, P. Horcajada-Cortes, G. Férey, M. Daturi and Y.-K. Hwang, *U.S. Pat.*, US 2011/0172412 A1, 2011.
58 Y. He, Z. Zhang, S. Xiang, F. R. Fronczek, R. Krishna and B. Chen, *Chem. Commun.*, 2012, **48**, 6493–6495.
59 S. H. Hyun and R. P. Danner, *J. Chem. Eng. Data*, 1982, **27**, 196–200.
60 N. Lamia, M. A. Granato, P. S. Gomes, C. A. Grande, L. Wolff, P. Leflaive, D. Leinekugel-le-Cocq and A. E. Rodrigues, *Sep. Purif. Technol.*, 2009, **44**, 1485–1509.
61 A. Anson, Y. Wang, C. C. H. Lin, T. M. Kuznicki and S. M. Kuznicki, *Chem. Eng. Sci.*, 2008, **63**, 4171–4175.
62 P. D. C. Dietzel, R. Blom and H. Fjellvåg, *Eur. J. Inorg. Chem.*, 2008, 3624–3632.
63 S. R. Caskey, A. G. Wong-Foy and A. J. Matzger, *J. Am. Chem. Soc.*, 2008, **130**, 10870–10871.
64 P. D. C. Dietzel, Y. Morita, R. Blom and H. Fjellvåg, *Angew. Chem., Int. Ed.*, 2005, **44**, 6354–6358.
65 W. Zhou, H. Wu and T. Yildirim, *J. Am. Chem. Soc.*, 2008, **130**, 15268–15269.
66 S. S.-Y. Chui, S. M.-F. Lo, J. P. H. Charmant, A. G. Orpen and I. D. Williams, *Science*, 1999, **283**, 1148–1150.
67 D. Sun, S. Ma, J. M. Simmons, J.-R. Li, D. Yuan and H.-C. Zhou, *Chem. Commun.*, 2010, **46**, 1329–1331.
68 Y. Hu, S. Xiang, W. Zhang, Z. Zhang, L. Wang, J. Bai and B. Chen, *Chem. Commun.*, 2009, 7551–7553.
69 X. Lin, J. Jia, X. Zhao, K. M. Thomas, A. J. Blake, G. S. Walker, N. R. Champness, P. Hubberstey and M. Schröder, *Angew. Chem., Int. Ed.*, 2006, **45**, 7358–7364.
70 X. Lin, I. Telepeni, A. J. Blake, A. Dailly, C. M. Brown, J. M. Simmons, M. Zoppi, G. S. Walker, K. M. Thomas, T. J. Mays, P. Hubberstey, N. R. Champness and M. Schröder, *J. Am. Chem. Soc.*, 2009, **131**, 2159–2171.
71 Z. Guo, H. Wu, G. Srinivas, Y. Zhou, S. Xiang, Z. Chen, Y. Yang, W. Zhou, M. O'Keeffe and B. Chen, *Angew. Chem., Int. Ed.*, 2011, **50**, 3178–3181.
72 B. Chen, N. W. Ockwig, A. R. Millward, D. S. Contreras and O. M. Yaghi, *Angew. Chem., Int. Ed.*, 2005, **44**, 4745–4749.
73 A. G. Wong-Foy, O. Lebel and A. J. Matzger, *J. Am. Chem. Soc.*, 2007, **129**, 15740–15741.
74 M. T. Ho, G. W. Allinson and D. E. Wiley, *Ind. Eng. Chem. Res.*, 2008, **47**, 4883–4890.
75 R. Kumar, *Ind. Eng. Chem. Res.*, 1994, **33**, 1600–1605.
76 R. Krishna and J. R. Long, *J. Phys. Chem. C*, 2011, **115**, 12941–12950.
77 R. Krishna and J. M. van Baten, *Sep. Purif. Technol.*, 2012, **87**, 120–126.
78 R. Krishna and R. Baur, *Sep. Purif. Technol.*, 2003, **33**, 213–254.
79 A. L. Myers and J. M. Prausnitz, *AIChE J.*, 1965, **11**, 121–127.

